World Electric Vehicle Journal

MDPI

Article

Lightweight Type-IV Hydrogen Storage Vessel Boss Based on Optimal Sealing Structure

Weidong Shao, Jing Wang *, Donghai Hu, Dagang Lu and Yinjie Xu

School of Vehicle and Traffic Engineering, Jiangsu University, Zhenjiang 212013, China; 2232104004@stmail.ujs.edu.cn (W.S.); 1000004735@ujs.edu.cn (D.H.); 2112304071@stmail.ujs.edu.cn (D.L.); 2222204005@stmail.ujs.edu.cn (Y.X.)

* Correspondence: 1000004847@ujs.edu.cn

Abstract: The seal and weight of the Type IV hydrogen storage vessel are the key problems restricting the safety and driving range of fuel cell vehicles. The boss, as a metal medium connecting the inner liner of the Type IV hydrogen storage vessel with the external pipeline, affects the sealing performance of the Type IV hydrogen storage vessel, and there is no academic research on the weight of the boss. Therefore, according to the force characteristics of the boss, this paper divides the upper and lower areas (valve column and plate). The valve column with seal optimization and light weight is manufactured with a 3D printing additive, while the plate bearing and transferring the internal pressure load is manufactured by forging. Firstly, a two-dimensional axisymmetric simulation model of the sealing ring was established, and the effects of different compression rates on its seal performance were analyzed. Then, the size and position of the sealing groove were sampled, simulated, and optimized based on the Latin Hypercube method, and the reliability of the optimal seal structure was verified by experiments. Finally, the Solid Isotropic Material with Penalization (SIMP) topology method was used to optimize the weight of the boss with optimal sealing structure, and the reconstructed model was checked and analyzed. The results show that the weight of the optimized boss is reduced by 9.6%.

Keywords: type IV hydrogen storage vessel; boss; sealing performance; lightweight

Citation: Shao, W.; Wang, J.; Hu, D.; Lu, D.; Xu, Y. Lightweight Type-IV Hydrogen Storage Vessel Boss Based on Optimal Sealing Structure. *World Electr. Veh. J.* **2024**, *15*, 261. https://doi.org/10.3390/wevj15060261

Academic Editor: Joeri Van Mierlo

Received: 26 May 2024
Revised: 11 June 2024
Accepted: 12 June 2024
Published: 15 June 2024

1. Introduction

As a key component of fuel cell vehicles, the safety and reliability of the Type IV hydrogen storage vessel are crucial [1–3]. As a key sealing component of the Type IV hydrogen storage vessel, the boss directly affects hydrogen leakage. Therefore, through the analysis and optimization of the material and structure of the boss, the sealing performance of the Type IV hydrogen storage vessel under high-pressure conditions can be improved, and the number of hydrogen filling and discharging times of the Type IV hydrogen storage vessel can be increased to extend the service life [4–8]. In addition, the mass of the boss can be reduced as much as possible to meet the design requirements. On the one hand, the boss can reduce the overall quality of the Type IV hydrogen storage vessel, increase the hydrogen storage density, and improve the mileage; on the other hand, it can reduce the inertia of the Type IV hydrogen storage vessel, reduce the impact force during collision, and improve the safety of the Type IV hydrogen storage vessel [9–13]. Therefore, under the background of the continuous development of hydrogen energy technology, the research on the sealing and lightweight design of the boss will provide a solid guarantee for the sustainable development and promotion of fuel cell vehicles.

2. Literature Review and Research Ideas

In order to ensure the safe and stable operation of the Type IV hydrogen storage vessel, scholars have performed many studies on the boss. Zhu [14] studied the effects

of high-performance materials on the boss, the angle of the rotating platform, and the number of sealing slots on its strength, fatigue, and sealing performance and proposed an optimized boss structure to further ensure the safety of hydrogen storage vessels. Motaharinejad et al. [15,16] studied the influence of the surface treatment of the boss on its adhesion to the inner liner. A method of sandblasting combined with a PEG coating was proposed to improve the service life of hydrogen storage vessels. Li [17] studied the influence of the temperature field of the boss during the rapid hydrogenation process and proposed an optimal hydrogenation strategy to reduce the deformation and stress concentration of the hydrogen storage vessel. Although scholars have studied the mechanics, welding, and temperature field of the boss, there are few studies on the sealing performance of the boss, especially studies of high-pressure hydrogen being more likely to leak and lead to explosions, fire, and other serious consequences.

Under the condition of meeting the safety and reliability of Type IV hydrogen storage vessels, the weight of the vessel can be effectively reduced so as to improve the hydrogen storage density and increase the driving range, so a lightweight Type IV hydrogen storage vessel has attracted the attention of researchers. Wang et al. [18–20] studied the influence of the carbon fiber winding angle on the reinforcement layer thickness of hydrogen storage vessels and determined the optimal winding angle parameter through an optimization algorithm to achieve lightweight effects for hydrogen storage vessels. Ellul et al. [21–23] studied the effect of the reinforcement layer sequence on the surface deformation and fracture of the hydrogen storage vessel and achieved a strengthening effect by obtaining the global optimal result. Paknahad et al. [24–26] used the inertial weight particle swarm optimization algorithm to optimize the head profile of the filament-wound composite pressure vessel and obtained a dome head with high shape coefficient and light weight. Although a lot of research has been conducted on the reinforcement layer and liner weight optimization of the Type IV hydrogen storage vessel, there is no academic research on the weight of the boss.

In view of the above research deficiencies, this paper carries out the following work:

(1) In order to improve the reliability of the sealing structure, a two-dimensional axisymmetric model of the sealing structure was established, the compression ratio range of the sealing ring suitable for the sealing structure was determined by simulation, the influence of the size and position of the sealing groove on the mechanics of the boss was analyzed, and the sealing design parameters were optimized.

(2) In order to reduce the weight of the boss, the optimal sealing parameters were selected to design and analyze the mechanical response of the boss. The lightweight design was carried out based on SIMP topology optimization, and the model reconstruction and check analysis were carried out on the lightweight results of the boss.

As shown in Figure 1, the overall design flowchart of this study includes sealing structure design and simulation analysis of the boss, parameter optimization analysis, and topology optimization of the boss.

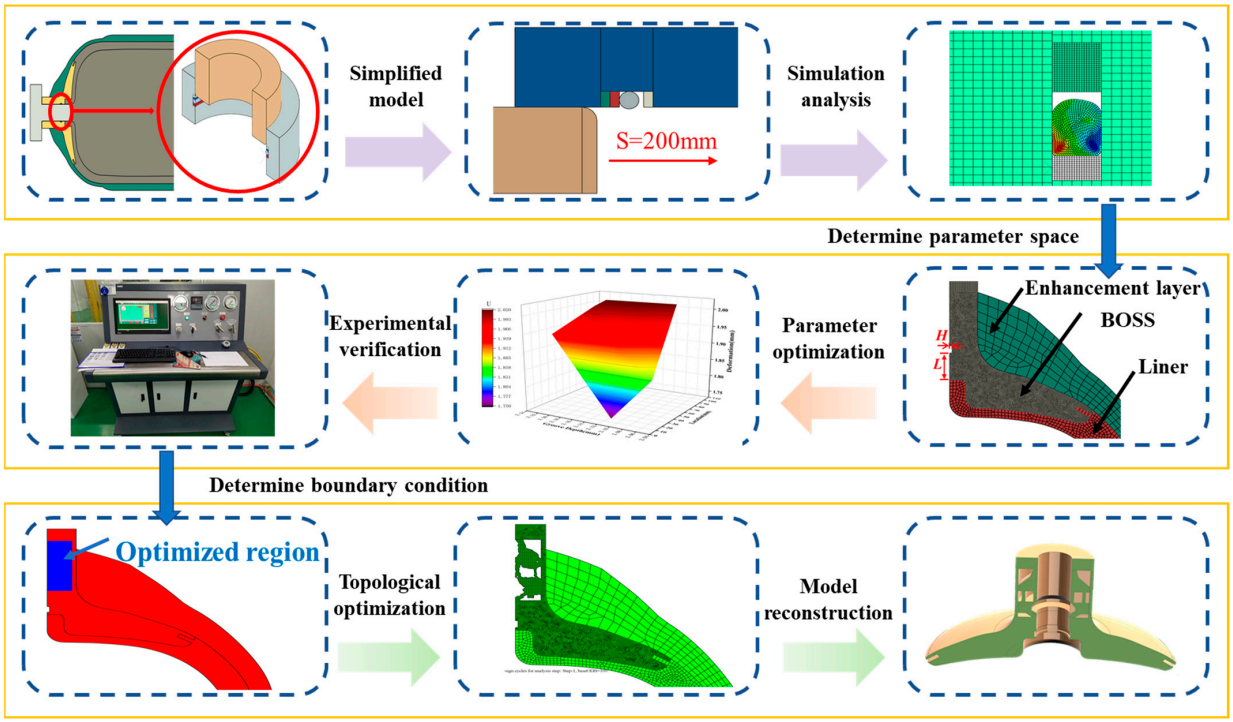

Figure 1. Flowchart of the overall idea of the paper.

3. Optimization and Verification of the Boss Seal Structure

3.1. Working Principle of Sealing Structure

Due to its small molecular diameter, hydrogen easily passes through the tiny pores of many materials [27,28]. Therefore, the sealing of the boss is an important factor affecting the safety of the hydrogen storage system. The sealing structure can be divided into shaft sealing and cylinder sealing according to the location of the sealing groove. The shaft seal is a sealing structure where the sealing groove is located on the seat, also known as the type II seal. The shaft seal is usually compact in design, occupies a small space, and is suitable for equipment and machinery with limited space. On the other hand, the shaft seal can maintain stable sealing at high temperatures or in corrosive environments to prevent hydrogen leakage [29,30]. In this paper, due to the complex structure of the valve and limited space, blindly opening a sealing groove on the valve will easily lead to insufficient strength of the valve. Therefore, the sealing structure of the hydrogen storage vessel is designed on the simple structure of the boss.

The sealing structure is generally composed of sealing ring, gasket, sealing groove, etc., as shown in Figure 2a,b. Common sealing ring structures include the O-sealing ring, Y-sealing ring, square sealing ring, and so on. The O-sealing ring is widely used in mechanical sealing mechanisms because of its simple structure, reliable operation, and good sealing performance. However, under the action of medium pressure, the sealing ring may squeeze into the gap between the installation groove and the sealing part, causing damage to the sealing ring and medium leakage. Therefore, when the working pressure is greater than 9.8 Mpa, the sealing structure in the design should consider increasing gaskets to avoid the O-sealing ring squeezing into the gap. Medium pressure is 70 MPa, so the gaskets are added around the sealing ring to ensure uniform pressure of the sealing ring and improve the service life. In the actual work, the correct match between the sealing ring and the sealing groove size is the key factor affecting the sealing effect, among which the most important design parameters are the compression rate and the groove filling rate. The compression rate of the sealing ring is generally recommended to be E = 10 ~ 25%, and the compression rate is appropriately adjusted according to the pressure in the vessel during normal operation. The maximum groove filling rate of the sealing ring should not exceed

90%; if the filling rate is too large, the permanent deformation of the sealing ring increases, and there may even be extrusion and cutting phenomena, resulting in the failure of the sealing ring. When the filling rate is too small, the sealing ring will move in the sealing groove in response to pressure changes, affecting the sealing effect. The best filling rate n = 70 ~ 85%. In this paper, the ideal filling rate n = 75% is selected. The final sealing structure parameters are shown in Table 1.

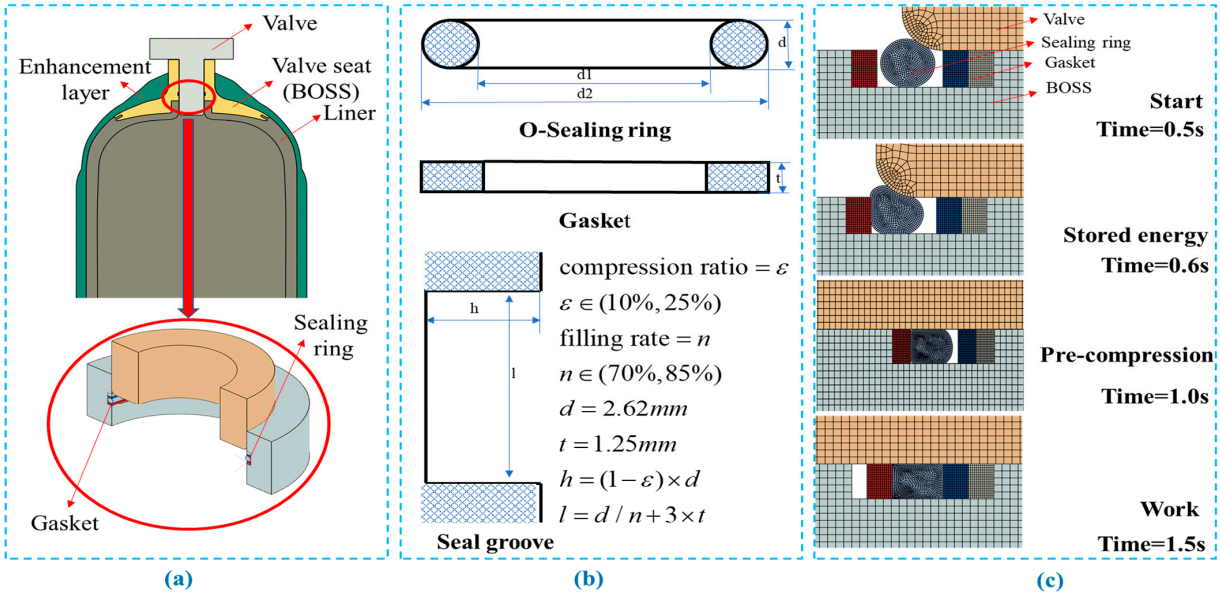

Figure 2. Seal structure working principle diagram: (**a**) Seal structure; (**b**) Seal part; (**c**) Working condition.

Table 1. Sealing component dimension.

Name of Parts	Parameter	Value	Units
Sealing ring	Inner diameter (d1)	32.5	mm
	Diameter (d)	2.62	mm
Gasket	Thickness (t)	1.25	mm
Sealing groove	Depth (h)	1.97 ~ 2.35	mm
	Length (l)	7.25	mm

The work of the sealing system can be divided into two processes: the pre-compression process of the sealing ring interference assembly and the sealing process of the hydrogen medium acting indirectly on the sealing ring, as shown in Figure 2c. The sealing ring can first be installed evenly and without distortion in the boss using appropriate lubricants to reduce friction. At this time, the sealing ring is in a natural state or subject to small external constraints or pressures. In this state, the shape and size of the sealing ring are basically in line with the elastic characteristics of its material. The valve is then slowly pushed into the boss, and the chamfer area at the front of the valve contacts the sealing ring to guide it to correct deformation until the overall compression. At this time, the shape and size of the sealing ring changes significantly; due to the elasticity of the sealing ring material, it will store a certain amount of elastic potential energy, which can also be called the energy storage process. Finally, the hydrogen medium in the vessel acts on the gasket and then compresses the sealing ring, increasing the contact pressure between the sealing ring and the valve. When the contact pressure is larger than the medium pressure, the whole system completes the efficient and reliable sealing task.

3.2. Seal Simulation Analysis

3.2.1. Establishment of Sealing Model

The traditional sealing structure design is generally based on previous project experience, and the design efficiency is low and the effectiveness cannot be guaranteed. In recent years, finite element simulation analysis has been widely used in the research of sealing structures, which has greatly reduced the number of samples and related tests and shortened the product development cycle [31,32]. The material of the sealing ring used in this paper is Ethylene Propylene Diene Monomer (EDPM), which has the characteristics of low density and heat resistance and is a super-elastic material. Since the loading and deformation behavior of EDPM is nonlinear, a special material model is required for accurate simulation and analysis of the rubber model [33], so this paper uses the Mooney–Rivlin model to simulate its material characteristics. The model can well describe the stress–strain and deformation behavior of rubber materials under different loading conditions and can provide practical simulation results. The formula of the two-parameter Mooney–Rivlin model is as follows:

$$W = C_{10}(I_1 - 3) + C_{01}(I_2 - 3) \quad (1)$$

where W is the strain energy density function, I_1 and I_2 are the first and second strain invariants, respectively, and C_{10} and C_{01} are the mechanical property constants. The Mooney–Rivlin coefficients C_{10} and C_{01} of rubber materials directly affect the stress distribution of the sealing ring, and the parameters can be obtained by uniaxial tensile test of the rubber samples and curve fitting in MATLAB. The EDPM material parameters are shown in Table 2.

Table 2. EDPM mechanical parameters.

Parameter	Value	Units
Specific Gravity	1.18	g/cm^3
Hardness (shore A)	94	Point
Elongation at Break	181	%
Tensile Strength	22.26	MPa
C_{10}	1.4	\
C_{01}	0.35	\

In this paper, ABAQUS finite element analysis software is used to establish a two-dimensional axisymmetric finite element model of the O-sealing ring. The basic assumptions are as follows: (1) The elastic modulus of the boss, valve, and gasket is tens of thousands of times that of rubber and can be regarded as a rigid body structure. (2) The rubber sealing ring material is regarded as an incompressible material, so the Poisson ratio of the rubber material is 0.5. (3) The sealing structure of the rubber sealing ring is handled according to the axisymmetric problem.

The simulation condition is divided into two analysis steps: the sealing ring assembly and the hydrogen medium action. In the assembly process, due to the use of lubricants to protect the sealing ring, the hard contact friction coefficient is less than the general rubber and metal friction coefficient, which is set at 0.25 for this paper. The boss is fully restrained during assembly, and the valve is shifted down the axis by 200 mm. When the sealing ring is working, it will withstand 70 MPa, so in the second analysis step, the medium pressure load is increased to act on the gasket.

3.2.2. Analysis of Sealing Simulation Results

As the compression rate of the sealing ring has a great impact on the sealing performance of the structure, the current sealing ring manufacturers generally recommend the range of the compression rate of the sealing ring, and the specific ideal value is affected by the contact material and media pressure, so this paper designs the control variable simulation according to the compression rate of the sealing ring. The size of the sealing ring is limited by the manufacturer's mass production and is not easy to change. Therefore, this

paper changes the compression rate of the sealing ring by changing the depth of the sealing groove (H) and selects the compression rate E = 10%, 15%, 18%, 20%, 22%, 25%, and the corresponding sealing groove depth H = 2.35, 2.22, 2.15, 2.10, 2.04, 1.97 mm, respectively. To analyze its sealing performance and failure risk during pre-compression and operation, the parameters related to the seal characteristics of the system are contact length during pre-compression and contact pressure and effective contact length after the application of medium pressure; contact pressure and rubber seal material failure can be judged according to the maximum shear stress strengthening theory.

As shown in Figure 3a, when the sealing ring is in the pre-compression process, the contact pressure of the sealing surface shows a trend that the value of the left side is lower than that of the right side, the pressure peak appears on the right side of the midpoint of the contact surface, and the pressure drop rate on the right side is higher than that on the left side. At the same time, as the compression rate of the sealing ring increases, the amplitude, average value, and contact length of the contact pressure also increase. During the pre-compression process, the minimum contact pressure amplitude and contact length of the sealing ring appear at the compression rate E = 10%, with 7.5 MPa, and 1.02 mm, respectively, while the maximum contact pressure amplitude and length appear at the compression rate E = 25%, with 18.5 MPa and 2.01 mm, respectively. As shown in Figure 3b, due to the large deformation of the sealing ring under medium pressure, the contact pressure of the sealing surface becomes constantly rising, and the amplitude appears on the far right of the contact surface. At the same time, as the compression rate of the sealing ring increases, the effective contact length evolves from a point to an increasingly longer straight line. During the sealing process, the minimum contact pressure amplitude and effective length appear at the compression rate E = 10%, which are 72.0 MPa and an effective point (point A), while the maximum contact pressure amplitude and effective length appear at the compression rate E = 25%, which are 89.2 MPa and 2.16 mm, respectively.

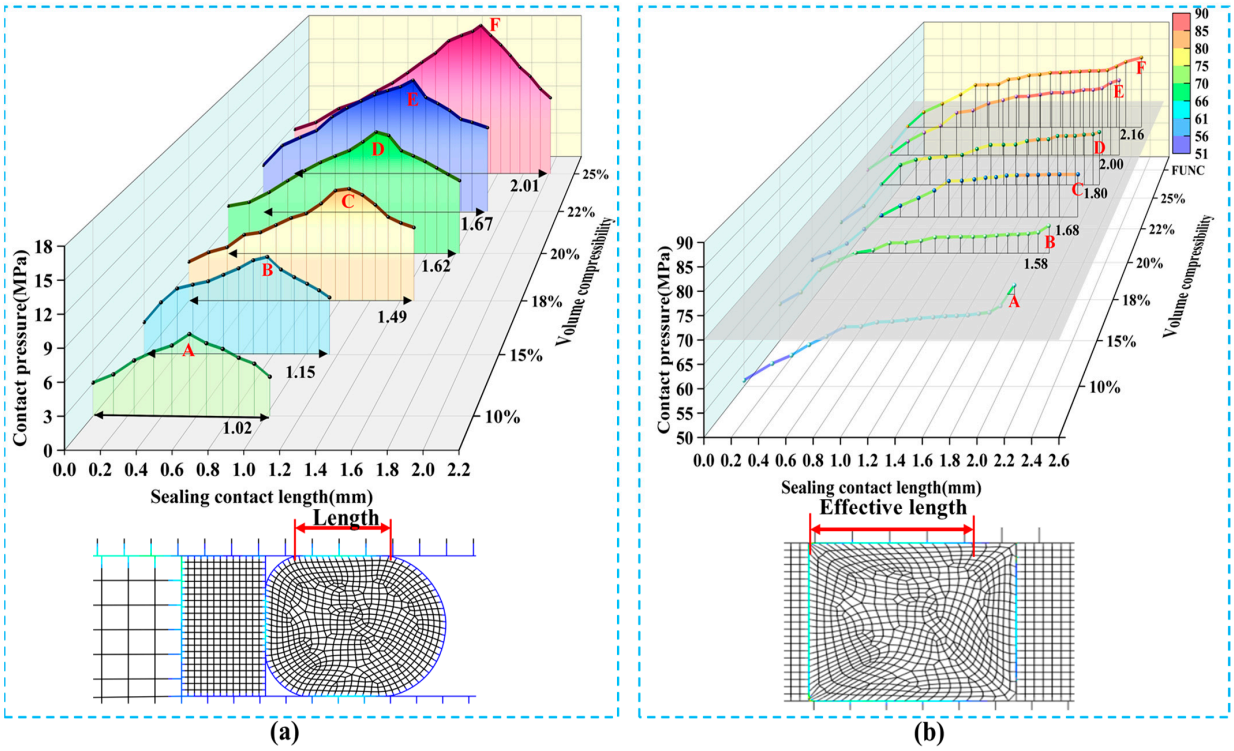

Figure 3. Different compression rates change the contact pressure of the sealing ring: (**a**) The contact pressure of the sealing ring during pre-compression; (**b**) The contact pressure of the sealing ring during work.

The simulation results of the sealing system show that with the increase in the compression rate of the sealing system, the contact pressure and length of the pre-compression process and the sealing process are increased, and the sealing performance is significantly improved. However, when the compression rate E = 10%, although the sealing stress is greater than the medium pressure, the effective length of the sealing contact is only one point, the reliability and stability of the sealing system are greatly reduced, and it is easy to cause hydrogen leakage and the scheme needs to be abandoned.

The sealing ring material used in this paper is EDPM, and the allowable shear strength of the sealing ring during the pre-compression process is 5.4 MPa. To ensure that the sealing material has sufficient strength, the safety factor of 1.5 is adopted, so the maximum working stress of the sealing material is 3.6 MPa. As shown in Figure 4, since the valve squeezes the sealing ring into one side of the sealing groove through friction during assembly, the bottom of the sealing ring contacts and deforms with the gasket, and with the increase in the compression rate, the bottom contact surface becomes larger, because the friction caused by the compression deformation of the valve and the boss on both sides will increase with the increase in the compression rate and then increase the clamping force to drive the sealing ring's downward movement. The bottom contact surface of the sealing ring increases. The minimum shear stress of the sealing ring appears on the side of the boss, and the shear stress amplitude appears on the bottom of the valve contact and increases rapidly with the increase in the compression rate. The minimum and maximum stress amplitude are 1.73 MPa and 4.42 Mpa, respectively, and the corresponding compression rates are E = 10% and E = 25%.

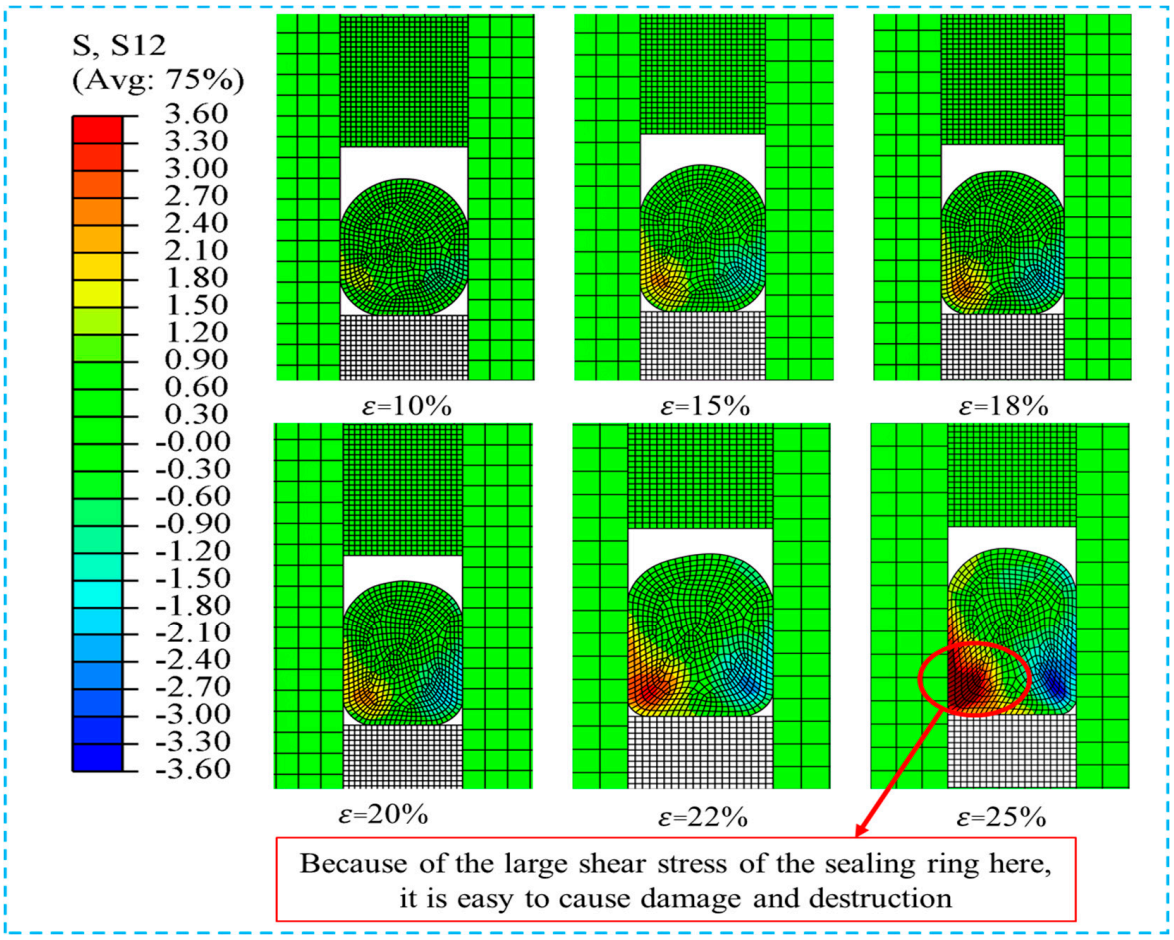

Figure 4. Sealing ring shear stress nephogram at different compression rates.

The simulation analysis shows that with the increase in the compression rate of the sealing structure, the shear stress of the sealing ring increases rapidly, and when the compression rate E = 25%, the shear stress of the lower left part of the sealing ring is concentrated and the stress in some areas exceeds the maximum stress of the material, which may lead to serious damage to the sealing ring and further reduce the sealing performance. Therefore, the compression rate scheme needs to be abandoned. When the compression rate of the sealing ring is E = 22%, the shear stress amplitude of this scheme is 3.24 MPa, and the risk of material damage and failure is small. In summary, according to the sealing performance and material damage failure analysis, this paper believes that the compression ratio suitable for this sealing system is E = 15 ~ 22%.

3.3. Optimization of Sealing Parameters

3.3.1. Establishment of Optimization Framework

The effect of the compression rate of the sealing ring on the sealing performance has been studied above, and the size and position of the sealing groove have an important impact on the mechanical properties of the boss. On the one hand, the position of the sealing groove affects the distribution of the load pressure inside the Type IV hydrogen storage vessel, and on the other hand, the stress concentration easily occurs at the corner of the sealing groove, which will affect the stress distribution and amplitude of the boss and the reinforcement layer. In this paper, two important parameters affecting the mechanical properties of the boss are selected: sealing groove depth (H) and position distance (L). In this paper, the Latin Hypercube Sampling [34] method is adopted for multi-dimensional parameter sampling. Latin Hypercube Sampling is a statistical sampling method used to select representative sample points in a multidimensional parameter space. This method is widely used in design experiments and simulations and can improve sampling efficiency, reduce errors, and maintain the uniformity and diversity of sampling.

(1) Determination of the parameter space, as shown in Figure 5a. H is affected by the above reasonable sealing structure compression rate E = 15 ~ 22%, so the range of H is 2.04 ~ 2.22 mm. The length of L is constrained by the position of the body thread, so the range of L is 0 ~ 100 mm.

(2) Uniform sampling, as shown in Figure 5b. The parameter space is evenly divided into 20 segments, and a random value is extracted from each segment parameter space. Finally, the sampling point is mapped to the specified side range.

(3) Model construction, as shown in Figure 5c. Based on the sample data, the 3D model of the boss is built, and the boundary conditions of the simulation model are set. The volume of the Type IV hydrogen storage vessel is 150 L. The boss is made of AL_6061, the inner liner is made of high polymer HDPE, and the reinforcement layer is made of T800s carbon fiber and phenolic resin composite with 60% fiber content. The layering winding method is a mixture of helical and hoop winding [35]. The helical winding angle is 12.72°, the total thickness of the helical winding is 8.47 mm, and the total thickness of the annular winding is 9.47 mm. The material simulation mechanical parameters of the type IV hydrogen storage bottle are shown in Table 3.

Table 3. Material parameters.

Materials	Density (g/cm^3)	Young's Modulus (GPa)	Poisson's Ratio	Yield Stress (MPa)
AL_6061	2.7	69	0.33	55.6
HDPE	0.95	0.93	0.38	25.48
T800s	1.62	179	0.3	2860

(4) Analysis of the results is shown in Figure 5d. The simulation results of one of the sealing structures with a moderate position were selected for analysis. The boss can be roughly divided into the two areas of valve column A and plate B. Due to the large thickness of region B and the outer carbon fiber reinforcement layer overlay, the internal

stress is transferred to the carbon fiber layer through plate B, so the overall deformation is small. For the boss stress, since plate B is not the main bearing part, the analysis amplitude is not of great significance, so the amplitude proportion is used in this paper to represent the influence of the design variables.

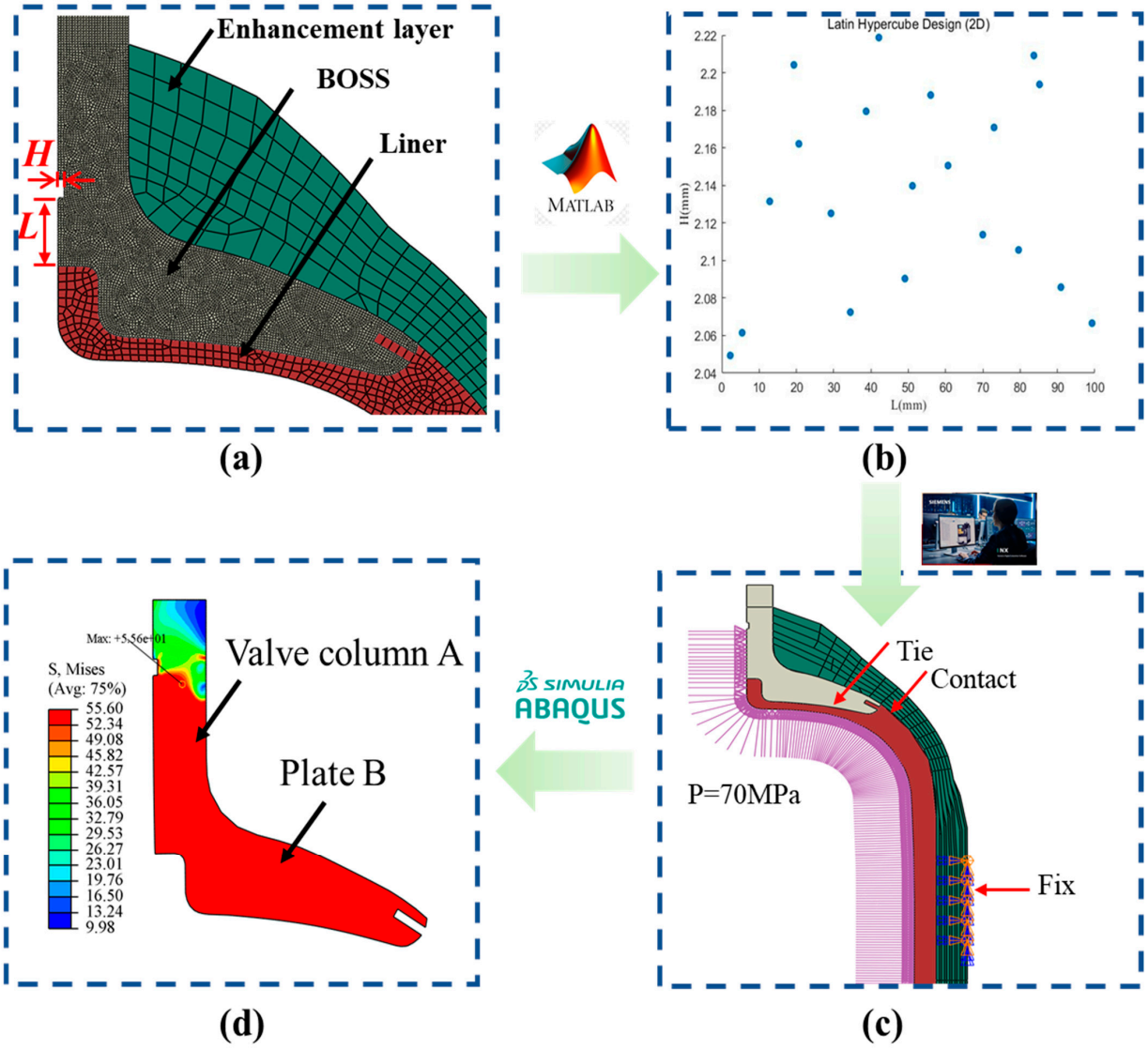

Figure 5. Sealing groove size and position optimization process: (**a**) Parameter selection; (**b**) Parameter sampling; (**c**) Simulation result; (**d**) Condition setting.

3.3.2. Analysis of Optimization Results

Shown in Figure 6a are the response surface of the maximum deformation and the design parameters. The maximum deformation will rise rapidly with the increase in the depth and position of the sealing groove, and the maximum deformation U = 2.02 appears at the maximum design parameter, that is, H = 2.24 and L = 100. Shown in Figure 6b are the response surface of the stress amplitude ratio and the design parameters. The response surface of the stress amplitude ratio shows that the amplitude proportion increases rapidly with the increase in the distance of the sealing groove, but when L = 50 ~ 65, the response surface rises gently, close to the plane, and when L > 65, the response surface rises rapidly, and the maximum value is 79%. Through the analysis of the response surface, when H = 2.98 and L = 6, the proportion of deformation and stress amplitude of the boss is small, so this scheme is chosen as the sealing structure design with the best mechanical properties of the boss.

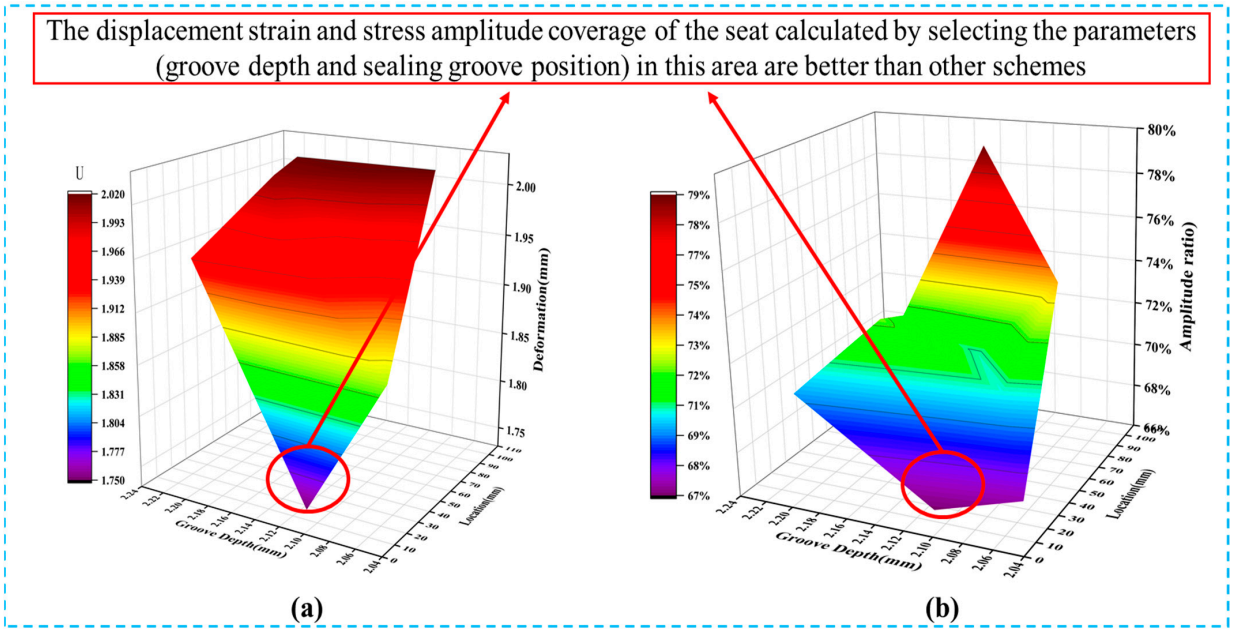

Figure 6. Influence law of sealing groove design parameters: (**a**) U-Parameter response surface; (**b**) Stress-Parameter response surface.

In this paper, the displacement and stress nephogram of the optimal design parameters and the initial parameters of the boss are compared. As shown in Figure 7a,c, after internal pressure is applied to the Type IV hydrogen storage vessel, the maximum deformation of the initial scheme occurs at the glue joint between the boss and the inner liner, and the amplitude is 1.84 mm. This is because the material of the inner liner is HDPE, and the modulus and stiffness of HDPE are much smaller than those of the metal material of the boss, so the boss bears the load at the glue place more than in other areas. After optimizing the design parameters, the maximum deformation position of the boss is at the outer chamfer of the boss, and the amplitude is 1.75 mm. This is because the design parameter H affects the distribution of the internal pressure load, and the internal pressure load surface on the optimized boss is very small and almost negligible, so the maximum deformation is mainly the extrusion strain generated by the winding of the external reinforcement layer. The stress comparison is shown in Figure 7b,d, where the stress amplitude of the boss is mainly located in panel B and the amplitude is 55.6 MPa. This is because the main loading component of the Type IV hydrogen storage vessel is the reinforcement layer. With the linear increase in the internal pressure load, the stress at plate A easily reaches the yield stress of the material, and the rest of the load is transferred to the reinforcement layer through the plate. The valve column A will only be subjected to the small extrusion pressure of the reinforcement layer, so the stress at the valve column A is small, and the material properties are not fully played.

By optimizing the design parameters, the deformation amplitude of the boss is significantly reduced, and the location of the amplitude is improved. The stress amplitude proportion of the boss is reduced, and the stress at the valve column A is also reduced. This shows that after optimizing the design parameters of the sealing groove, the stress distribution of the boss is more uniform, the stress at the valve column A is effectively reduced, and the reliability and stability of the boss are improved, which is conducive to the subsequent lightweight design of valve column A.

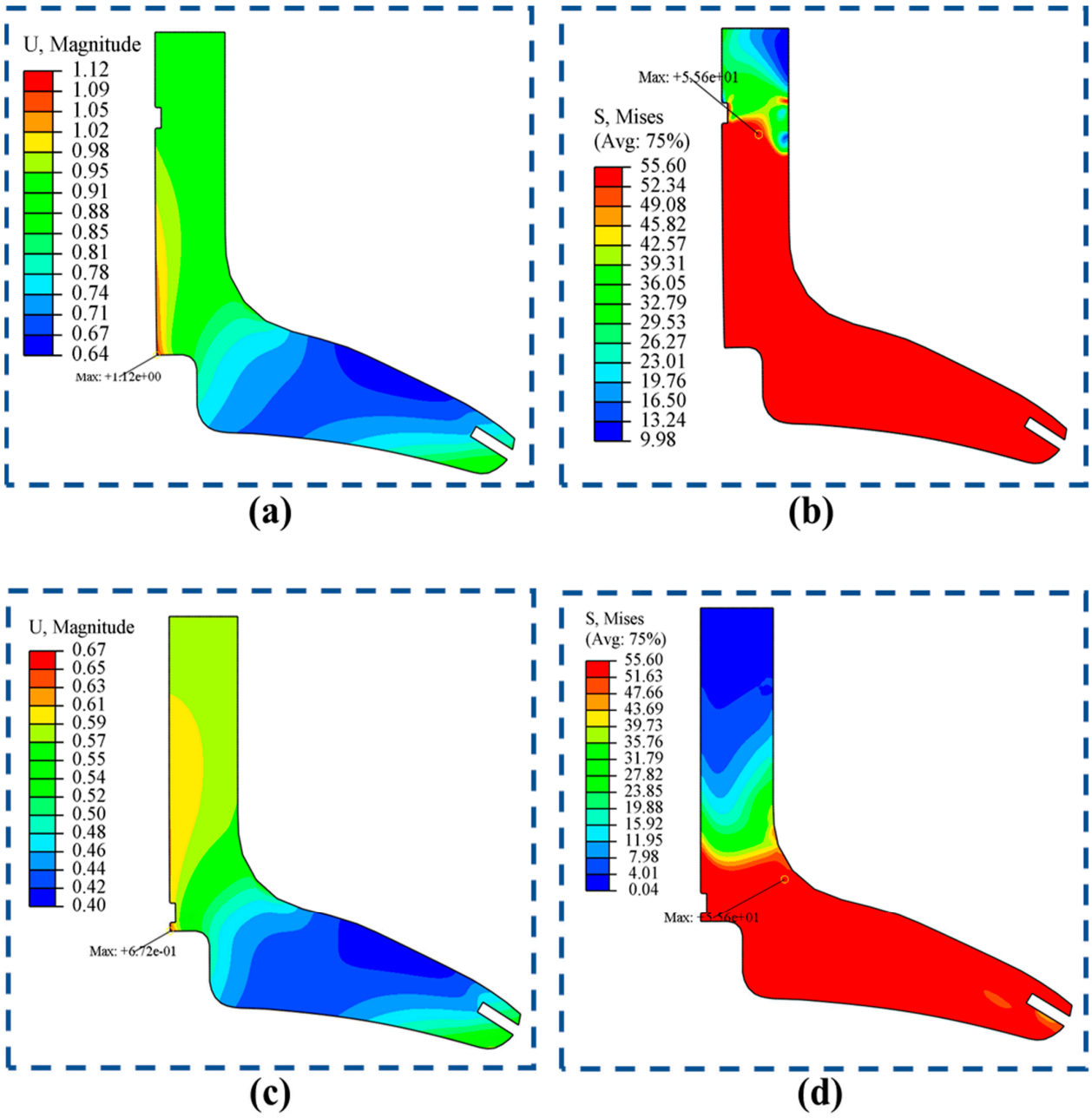

Figure 7. Comparison of sealing groove design before and after optimization: (**a**) Deformation of the initial solution for the boss; (**b**) Stress of the initial solution for the boss; (**c**) Deformation of the optimal solution for the boss; (**d**) Stress of the optimal solution for the boss.

3.4. Experimental Verification

In order to verify the sealing effectiveness of the optimal sealing structure of the boss, this paper conducted sealing leak detection experiments and damage detection experiments for the sealing structure. The experimental platform is shown in the Figure 8. The experimental platform established in this paper is based on the T/CMES 16003-2021 high-pressure hydrogen storage system hydrogen pressure cycle test and leakage/penetration test methods. The specific equipment is as follows. (1) Experimental helium cylinder tank: it provides helium for the experimental sealing system. (2) Pneumatic gas booster console: it is mainly composed of booster pump and control platform, which can detect and control experimental helium pressure in real time. (3) Gas leak detection test bench: tests the experimental seal structure with the bubble detection method. (4) Seal damage

detection platform: determines or measures seal damage through high-precision quadratic projector. Firstly, plugs are used to plug the exhaust port on the test piece, the booster pump pipeline and the valve intake port are connected, and it is ensured that there is no leakage at the import and export of the test device. Then, the helium gas is pressurized to 1.15 times the nominal pressure of the cylinder, that is 80.5 MPa, by the booster pump, and the pressurization is maintained during the test leak detection. Then, the specimen is immersed in the gas leak detection platform; all bubble leakage points, bubble diameter, and bubble rate are recorded; and the average value of three experimental records is taken. Finally, the experimental sealing ring is placed under the high-precision two-dimensional quadratic projector to observe the damage.

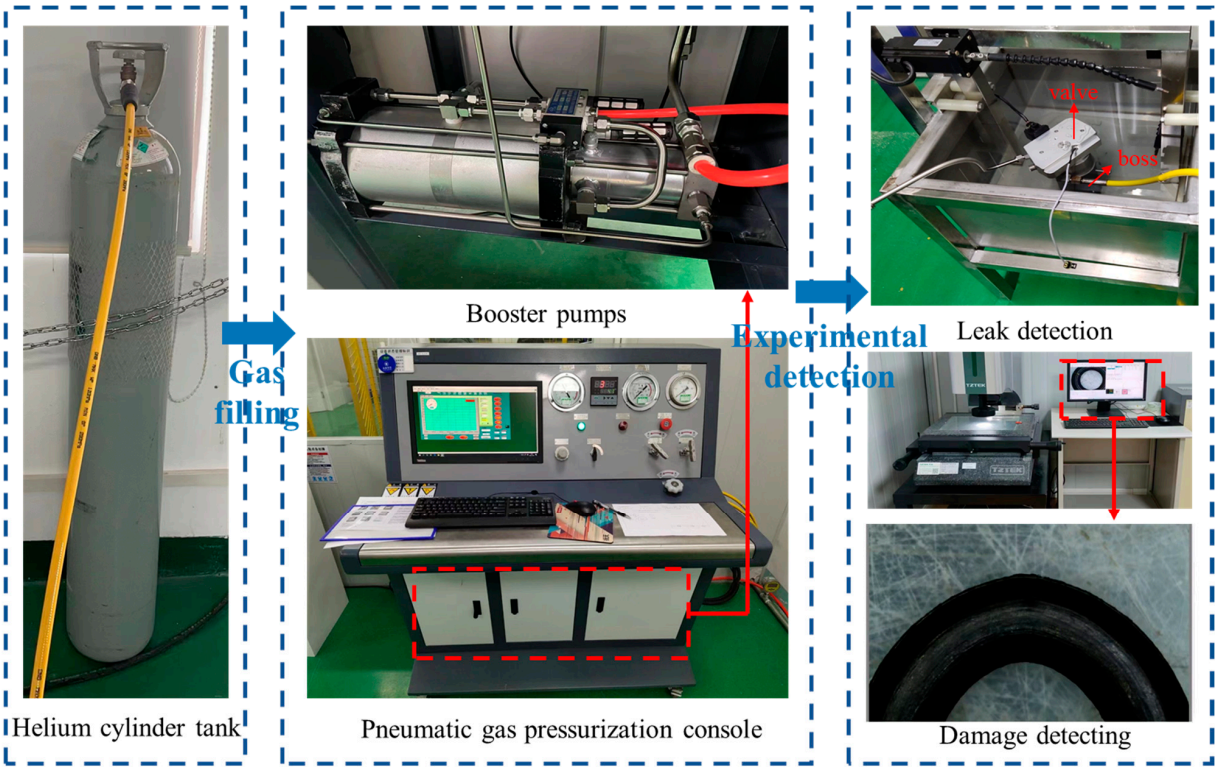

Figure 8. Experimental diagram of sealing structure of the boss.

The gas leakage points, leakage bubble diameters, and rates of test specimens were recorded, as shown in Table 4. The number of leakage points was two, the average bubble diameter was 3.7 mm, and the rate was 20 n/min. The comparison standard was that the bubble diameter was less than 5 mm and the allowable bubble rate was 50 n /min. The test did not exceed the limit values, and the sealing performance of the specimen was qualified. The damage result of the sealing ring under the high-precision two-dimensional projector is shown in Figure 8, and the sealing ring has no obvious gap, which is basically guaranteed to be intact. In summary, when the sealing structure is H = 2.98 and L = 6, the boss ensures the sealing reliability, and the sealing material is not damaged.

Table 4. Sealed test record table for leak detection.

Experiment	Leakage Point	Bubble Diameter (mm)	Bubble Rate (n/min)
1	2	3.6	22
2	2	3.2	24
3	1	4.4	13
mean value	2	3.7	20

4. Lightweight Boss Based on Optimal Sealing Structure

4.1. Establishment of Topology Optimization Model

Through the above simulation analysis, this paper finds the optimal sealing structure of the boss and determines the size and position of the sealing groove, which can help to carry out the topology optimization analysis of the boss. The lightweight design of parts can be achieved through shape, size, and topology optimization. However, the shape and size of the boss are limited by factors such as the inner liner and carbon fiber winding. In this paper, topology optimization is adopted to achieve the lightweight design of the boss. Topology optimization is a design method to determine the optimal structural type, which aims to minimize the weight of the structure while maintaining its performance and strength by redistributing the layout of materials and has been widely used in the field of engineering design [36,37].

In the stress cloud diagram of the optimal optimization scheme mentioned above, as shown in Figure 9a, the stress range of the valve column area is 3 ~ 20 MPa. Compared with the allowable stress of the boss metal, the overall stress is small and there is room for optimization. Therefore, the optimization area of region A is selected in this paper. Because the internal pressure can be reliably transferred to the carbon fiber reinforced layer, no optimization changes are made at the plate. Therefore, in this paper, the boss is divided into two parts, as shown in Figure 9b. Topology optimization is carried out in the valve column area, and additive manufacturing is carried out by 3D printing. The plate is mainly manufactured by integrated forging and cutting, and the upper and lower parts are connected by precision welding.

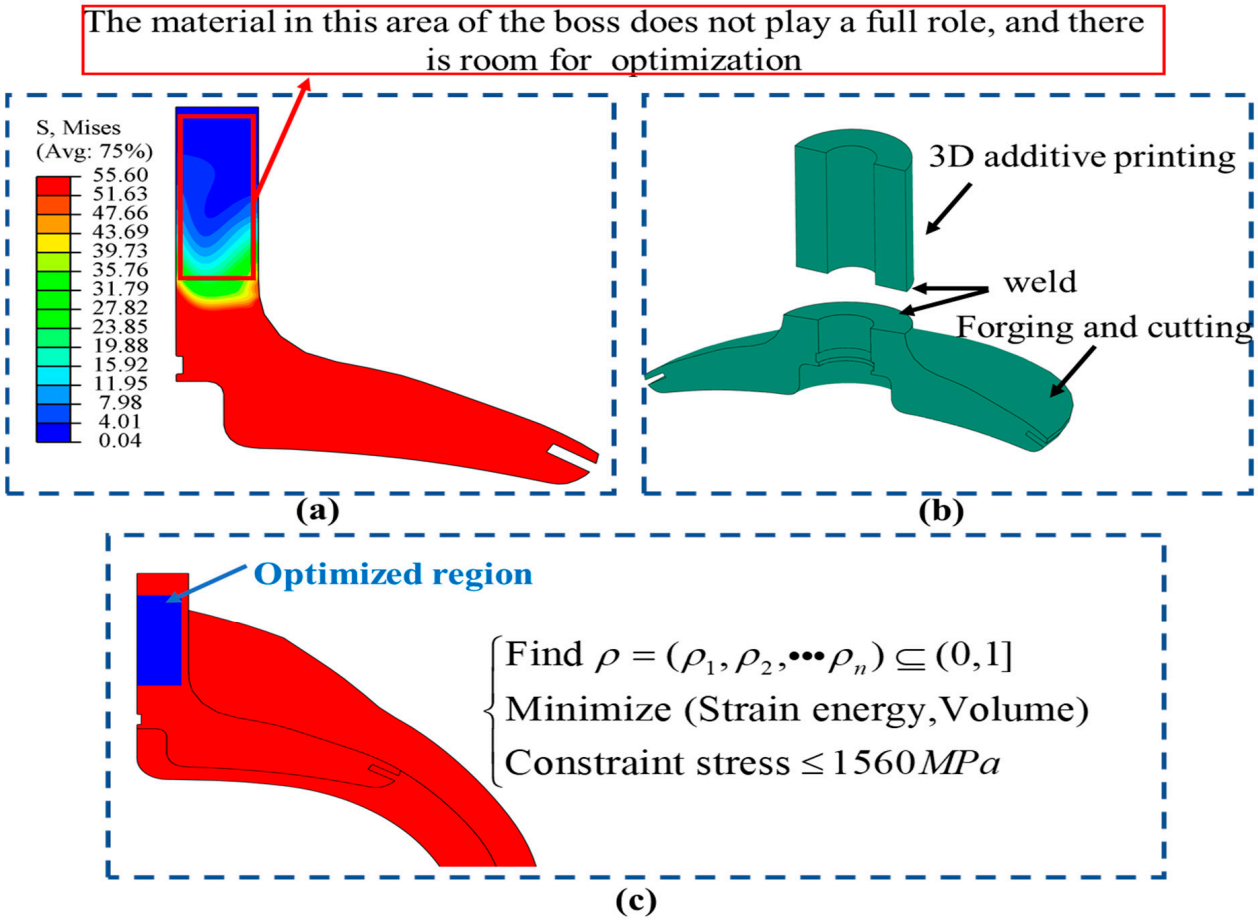

Figure 9. Topology optimization area and model: (**a**) Optimal parameter stress nephogram; (**b**) Manufacturing method; (**c**) Topology optimization model.

At present, the progressive structure method, variable density method, and homogenization method are commonly used in continuum topology optimization [38,39]. In this paper, the Solid Isotropic Material with Penalization (SIMP) in the variable density method is adopted. (1) The design variable of this method is the relative density (ρ_n) of each element, the value range is 0 ~ 1, and the continuous relative density distribution function is used. (2) Since the relative density of the material can be continuously changed, the Young's modulus of the material of each unit can also be continuously changed, and the specific formula is as follows. At the same time, the explicit expression of the geometric stiffness matrix of the plane element is derived by the Young's modulus of each element, and the geometric strain energy in the optimization criterion is obtained. (3) By analyzing the sensitivity of structural flexibility (reciprocal stiffness), volume, etc. to relative density, the density of each element of the part is iteratively optimized.

(4) The algorithm will eliminate the units and regions with density values close to 0 and retain the units and regions with density values close to 1.

$$E(\rho_n) = \rho_n^p E_0 \tag{2}$$

where p is the penalty factor and E_0 is the preset elastic modulus of the material.

As shown in Figure 9c, the weighted polynomial of the volume and strain energy of the topology optimization region is selected as the design target, with weighted values of 0.5 and 0.5. The design variable is the relative density of the cell, and the orientation ranges from 0.001 to 1. The constraint condition is that the maximum stress of the layer of the hydrogen storage bottle does not exceed 1660 MPa. By setting the penalty factor p to 3, the influence of the intermediate density elements on the total stiffness is reduced. The working load is consistent with the above hydrostatic simulation, and the region of applied load and boundary conditions is frozen.

4.2. Analysis of Topology Optimization Results

4.2.1. Iterative Result Analysis

As shown in Figure 10a, the optimization target of the iterative diagram of the topology optimization of the boss first rose rapidly, then slowly decreased and finally stabilized. This is because the initial density of the material is set to 0.5 and the stress could not meet the design requirements, so the rigid strength of the design area was improved by constantly increasing the material density of the optimized area, and the constraint conditions were gradually met. Meanwhile, as shown in Figure 10b, in the initial iteration, the optimization area did not change much. However, with the optimization iteration, the algorithm clearly abandoned the area with density close to 0, the outline of the topology scheme became more and more obvious, and the topology optimization scheme for the boss was finally obtained.

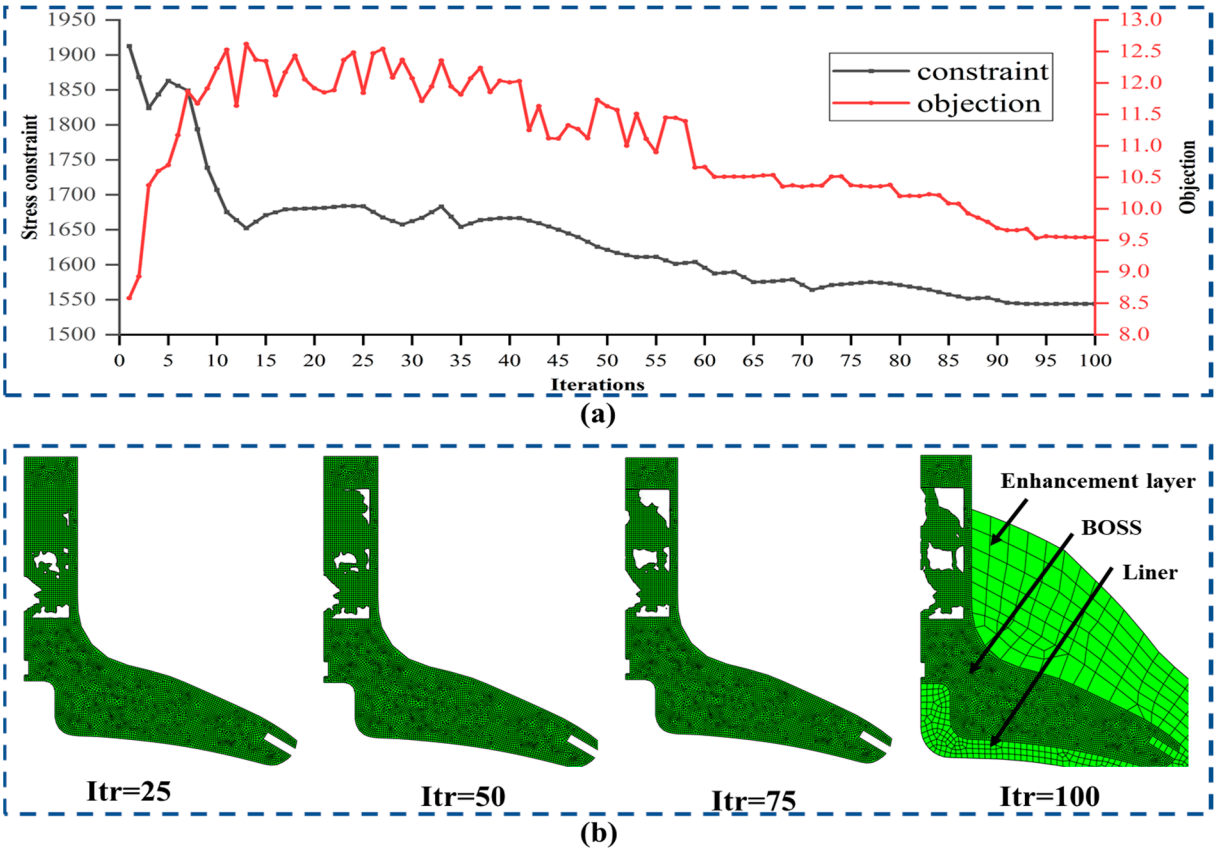

Figure 10. Iterative process of topology optimization: (**a**) Topology optimization iterative process data; (**b**) Topology optimization iteration results.

4.2.2. Reconstruction Model Check Analysis

After topological optimization, the structure of the boss does not need to remove much material, and the revision of the three-dimensional modeling should not have too much change to the initial modeling so as to avoid increasing the cost of technical transformation. Moreover, the processing technology should be fully implemented, and the model should be imported into the three-dimensional drawing software to correct and strengthen the force transmission path and obtain the reconstructed model. The reconfiguration model of the boss is shown in Figure 11a. After optimization, the mass of valve column A of the boss is reduced from 1.407 kg to 0.875 kg, a decrease of 37.8%, and the optimized mass accounts for 9.6% of the whole boss mass and the hydrogen storage density of the Type IV hydrogen storage vessel increased from 5.800 wt% to 5.871 wt%. However, whether the improved three-dimensional solid model can meet the safety strength requirements of the hydrogen storage vessel, it is necessary to check the perfect three-dimensional model again.

In order to verify the strength of the reconstructed model after topology optimization, finite element check analysis was re-performed on the boss part according to the relevant conditions and constraints above, and the finite element analysis results are shown in Figure 11b–d. In the simulation results, the overall stress amplitude of the hydrogen storage vessel is mainly concentrated in the reinforcement layer area outside the boss chamfering, and its amplitude reaches 1660 MPa, which is 120 MPa more than the 1540 MPa simulation result before optimization, but it meets the constraints of topology optimization and the strength of the lamination composite material. After the topological optimization design of the boss, the stress in the boss cylinder area increased significantly compared with that before optimization, and the deformation displacement also increased from 1.63 mm to 1.77 mm compared with the original model, but it still did not exceed the yield strain

range of the material. The results show that the topological optimization design not only improves the structural strength but also maintains the stability of the material.

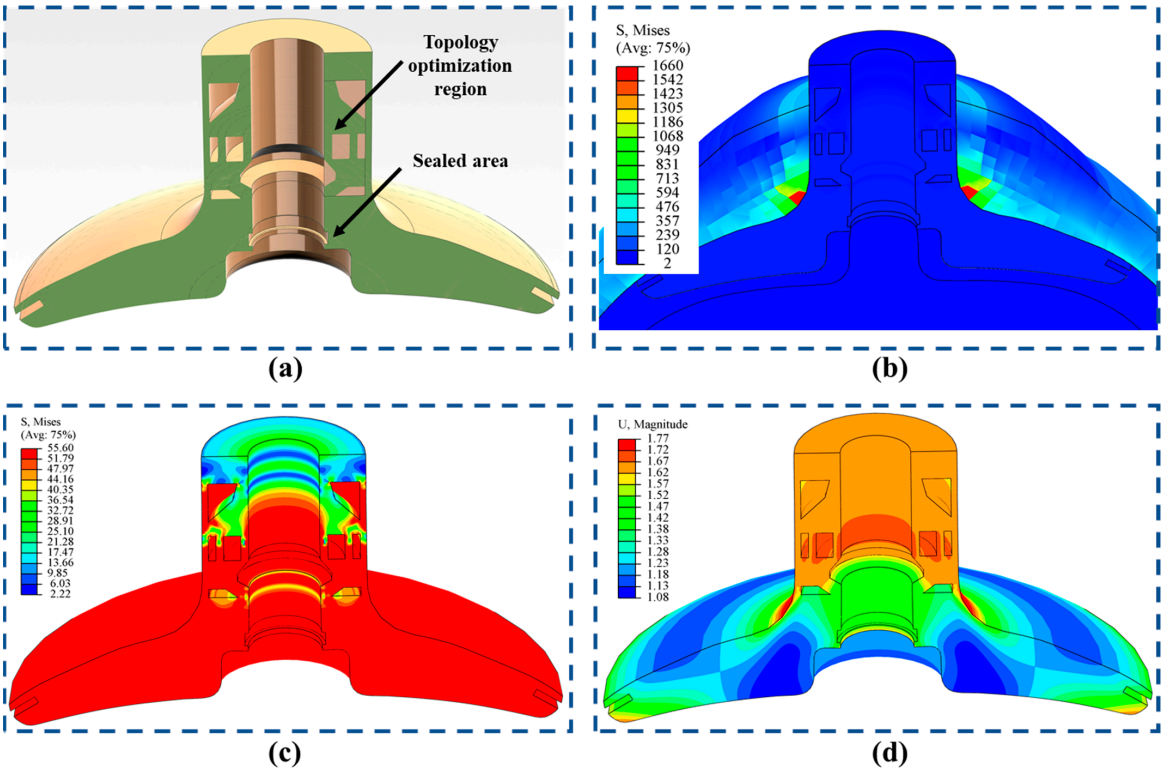

Figure 11. The verification results of the reconstructed model: (**a**) Topology optimization model reconstruction; (**b**) Stress nephogram of enhancement layer; (**c**) Stress nephogram of the boss; (**d**) Displacement nephogram of the boss.

5. Conclusions and Prospects

In order to solve the sealing failure problem of the Type IV hydrogen storage vessel boss and the requirement of light weight, the sealing ring and sealing groove sizes were designed according to the sealing requirements and material characteristics. Then, the effect of different compression rates on the sealing performance of the boss under the high pressure condition of 70 MPa was analyzed. Then, the effect of the size and position of the sealing groove on the mechanical properties of the boss is analyzed. Finally, the topology optimization design of the boss is carried out to meet the requirements of the boss design, and the reconstruction model is checked and analyzed.

The main conclusions of this paper are as follows:

(1) The compression rate of the sealing ring plays a key role in the sealing performance of the boss, and the contact pressure during the pre-compression process of the compression ratio is E = 10%, which is small. The effective contact length of the sealing ring is greater than the medium pressure and is only a point after the application of medium pressure in the sealing ring working process, and the sealing ring is prone to leakage. When the compression ratio is E = 25%, the shear stress of the sealing ring is too large, and the material is prone to damage and failure. Therefore, according to the sealing structure in this paper, the reasonable compression rate of the sealing ring is E = 15 ~ 22%. With the increase in the size and position of the sealing groove, the proportion of the deformation displacement and stress amplitude of the boss also increases. Therefore, the design scheme of H = 2.98 and L = 6 is selected according to the response surface in this paper to ensure the safety and stability of the boss to the greatest extent. Through the simulation analysis and optimization of the sealing ring and sealing groove, it provides reference for the design and optimization of the sealing and size shape of the boss.

(2) Through the topological optimization design and the check of the less stressed area of the boss, the overall mass of the boss was reduced by 0.53 kg, and the hydrogen storage density of the Type IV hydrogen storage vessel increased from 5.800 wt% to 5.871 wt%. This study fills a gap in the topology optimization design of the boss.

There are still two points that have not been studied in this paper. Further research directions are as follows:

(1) This paper only optimized the design of the boss and did not produce the topologically optimized boss by integrating 3D additive manufacturing and forging. Subsequent experimental testing of the boss' seal after lightweight design can be carried out.

(2) In order not to change the external shape, this paper adopts the topology optimization method to carry out the lightweight design of the boss. Based on the study on the stress and strain of the layering of the boss, a subsequent study can carry out the design of the boss's shape surface for the places where the stress concentration and deformation are large and enhance the application of new materials to optimize its stress distribution and further improve its safety and stability.

Author Contributions: Conceptualization, J.W.; methodology, J.W.; software, J.W.; validation, D.L.; formal analysis, W.S.; investigation, Y.X.; resources, D.L.; data curation, W.S.; writing—original draft preparation, W.S.; writing—review and editing, D.H.; visualization, Y.X.; supervision, D.H.; project administration, D.H.; funding acquisition, D.H. All authors have read and agreed to the published version of the manuscript.

Funding: This research was funded by the National Key Research and Development Program of China, "Integrated transportation and intelligent transportation" (2018YFB1600303).

Data Availability Statement: The original contributions presented in the study are included in the article, further inquiries can be directed to the corresponding author.

Conflicts of Interest: The authors declare no conflicts of interest.

References

1. Salehabadi, A.; Dawi, E.A.; Sabur, D.A.; Al-Azzawi, W.K.; Salavati-Niasari, M. Progress on nano-scaled alloys and mixed metal oxides in solid-state hydrogen storage; an overview. *J. Energy Storage* **2023**, *61*, 106722. [CrossRef]
2. Hu, D.; Wang, Y.; Li, J.; Yang, Q.; Wang, J. Investigation of optimal operating temperature for the PEMFC and its tracking control for energy saving in vehicle applications. *Energy Convers. Manag.* **2021**, *249*, 114842. [CrossRef]
3. Pugi, L.; Berzi, L.; Cirillo, F.; Vecchi, A.; Pagliazzi, V. A tool for rapid simulation and sizing of hybrid traction systems with fuel cells. *Proc. Inst. Mech. Eng. Part F J. Rail Rapid Transit* **2023**, *237*, 104–113. [CrossRef]
4. Hu, H.; He, Q.; Meng, Z. Analysis on safety of high-pressure hydrogen storage vessel in hydrogen fueling station. *Mod. Chem. Ind.* **2022**, *42*, 9–15.
5. Fang, Q.; Ji, D. Molecular simulation of hydrogen permeation behavior in liner polymer materials of Type IV hydrogen storage vessels. *Mater. Today Commun.* **2023**, *35*, 106302. [CrossRef]
6. Zhang, C.; Cao, X.; Bujlo, P.; Chen, B.; Zhang, X.; Sheng, X.; Liang, C. Review on the safety analysis and protection strategies of fast filling hydrogen storage system for fuel cell vehicle application. *J. Energy Storage* **2022**, *45*, 103451. [CrossRef]
7. Hu, D.; Hou, W.; Xiang, C.; Lu, D.; Yang, Q.; Li, J.; Wang, J. Waste heat utilization performance verification of Heat Exchanger Only Thermal Management System for fuel cell vehicle. *J. Clean. Prod.* **2023**, *428*, 139479. [CrossRef]
8. Duan, Z.; Mei, N.; Feng, L.; Yu, S.; Jiang, Z.; Chen, D.; Xu, X.; Hong, J. Research on hydrogen consumption and driving range of hydrogen fuel cell vehicle under the CLTC-P condition. *World Electr. Veh. J.* **2021**, *13*, 9. [CrossRef]
9. Yao, J.; Chen, X.; Lu, H.; Xu, Z.; Zhang, Z.; Liu, B. Dynamic response characteristics and damage modes of multifunctional layered hydrogen storage vessels under impact loads. *Int. J. Hydrogen Energy* **2024**, *54*, 526–539. [CrossRef]
10. Guo, Z.; Li, Z.; Cui, J.; Li, Y.; Luan, Y. The effect of winding patterns on the mechanical behavior of filament-wound cylinder shells. *Multidiscip. Model. Mater. Struct.* **2020**, *16*, 508–518. [CrossRef]
11. Park, W.R.; Jeon, S.K.; Kim, S.M.; Kwon, O. A study on the design safety of type III high-pressure hydrogen storage vessel. *J. Korean Soc. Saf.* **2019**, *34*, 7–14.
12. Zhang, C.; Gholipour, G.; Mousavi, A.A. State-of-the-art review on responses of RC structures subjected to lateral impact loads. *Arch. Comput. Methods Eng.* **2021**, *28*, 2477–2507. [CrossRef]
13. He, Q.; Li, X.; Mao, W.; Yang, X.; Wu, H. Research on Vehicle Frame Optimization Methods Based on the Combination of Size Optimization and Topology Optimization. *World Electr. Veh. J.* **2024**, *15*, 107. [CrossRef]
14. Zhu, J.; Li, Y.; Cao, W.; Li, Y.; Gao, Z. Failure Analysis of Novel BOSS Structures for Type IV Hydrogen Storage Vessels. *Energies* **2023**, *16*, 4005. [CrossRef]

15. Motaharinejad, V.; Delnaud, L.; Fouque, M.; Lucas, A.; Shirinbayan, M.; Fitoussi, J.; Tcharkhtchi, A. Enhancement of adhesion between the polymeric liner and the metallic connector of high-pressure hydrogen storage tank. *Int. J. Mater. Form.* **2021**, *14*, 249–260. [CrossRef]
16. Ahmadifar, M.; Benfriha, K.; Shirinbayan, M.; Aoussat, A.; Fitoussi, J. Exploring fatigue characteristics of metallic boss-polymer liner adhesion in hydrogen storage tanks: Experimental insights post surface treatment. *J. Energy Storage* **2024**, *75*, 109771. [CrossRef]
17. Li, J.; Liu, J.; Zhao, B.; Wang, D.; Guo, S.; Song, J.; Li, X. Research on Temperature Rise of Type IV Composite Hydrogen Storage Cylinders in Hydrogen Fast-Filling Process. *Energies* **2023**, *16*, 2918. [CrossRef]
18. Wang, Z.; Almeida, J.H.S., Jr.; Ashok, A.; Wang, Z.; Castro, S.G.P. Lightweight design of variable-angle filament-wound cylinders combining Kriging-based metamodels with particle swarm optimization. *Struct. Multidiscip. Optim.* **2022**, *65*, 140. [CrossRef]
19. Salavatian, M.; Smith, L.V. Matrix damage in composite pressure vessels with a bias fiber orientation. *J. Compos. Mater.* **2012**, *46*, 2793–2802. [CrossRef]
20. Lin, D.T.W.; Hsieh, J.C.; Chindakham, N.; Hai, P.D. Optimal design of a composite laminate hydrogen storage vessel. *Int. J. Energy Res.* **2013**, *37*, 761–768. [CrossRef]
21. Ellul, B.; Camilleri, D. The applicability and implementation of the discrete Big Bang-Big Crunch optimisation technique for discontinuous objective function in multi-material laminated composite pressure vessels. *Int. J. Press. Vessel. Pip.* **2018**, *168*, 39–48. [CrossRef]
22. Nebe, M.; Asijee, T.J.; Braun, C.; van Campen, J.; Walther, F. Experimental and analytical analysis on the stacking sequence of composite pressure vessels. *Compos. Struct.* **2020**, *247*, 112429. [CrossRef]
23. Madhavi, M.; Venkat, R. Predicting structural behavior of filament wound composite pressure vessel using three dimensional shell analysis. *J. Inst. Eng. (India) Ser. C* **2014**, *95*, 41–50. [CrossRef]
24. Paknahad, A.; Fathi, A.; Goudarzi, A.M.; Nourani, R. Optimum head design of filament wound composite pressure vessels using a hybrid model of FE analysis and inertia weight PSO algorithm. *Int. J. Mater. Form.* **2016**, *9*, 49–57. [CrossRef]
25. Hu, Z.; Chen, M.; Pan, B. Simulation and burst validation of 70 MPa type IV hydrogen storage vessel with dome reinforcement. *Int. J. Hydrogen Energy* **2021**, *46*, 23779–23794. [CrossRef]
26. Zu, L.; Xu, H.; Wang, H.; Zhang, B.; Zi, B. Design and analysis of filament-wound composite pressure vessels based on non-geodesic winding. *Compos. Struct.* **2019**, *207*, 41–52. [CrossRef]
27. Filippov, S.P.; Yaroslavtsev, A.B. Hydrogen energy: Development prospects and materials. *Russ. Chem. Rev.* **2021**, *90*, 627. [CrossRef]
28. Hassan, I.A.; Ramadan, H.S.; Saleh, M.A.; Hissel, D. Hydrogen storage technologies for stationary and mobile applications: Review, analysis and perspectives. *Renew. Sustain. Energy Rev.* **2021**, *149*, 111311. [CrossRef]
29. Huang, X.; Zhao, J.; Wang, Y.; Ke, Y.; Wang, Z. Study on a New Static Sealing Method and Sealing Performance Evaluation Model for PEMFC. *World Electr. Veh. J.* **2021**, *12*, 237. [CrossRef]
30. Song, Z.; Li, S.; Chen, X.; Liu, Z.; Zhao, T.; Huang, B. Study on the Service Performance of a Two-Stage Floating-Ring Isolation Seal for a High-Speed Turbopump with a Cryogenic Medium. *Machines* **2023**, *11*, 373. [CrossRef]
31. Zhang, L.; Wei, X. A novel structure of rubber ring for hydraulic buffer seal based on numerical simulation. *Appl. Sci.* **2021**, *11*, 2036. [CrossRef]
32. Wang, S.; Liu, P.; Li, D.; Dong, Z.; Li, G. Simulation and Experimental Study on Sealing Characteristics of Hydro-Pneumatic Spring GS Seal Rings. *Appl. Sci.* **2023**, *13*, 11703. [CrossRef]
33. Yang, H.U.; Zhang, J.; Chen, L.M. Design and seal performance analysis of bionic sealing ring for dynamic seal. *Mechanics* **2020**, *26*, 338–345.
34. Zhang, F.; Cheng, L.; Wu, M.; Xu, X.; Wang, P.; Liu, Z. Performance analysis of two-stage thermoelectric generator model based on Latin hypercube sampling. *Energy Convers. Manag.* **2020**, *221*, 113159. [CrossRef]
35. Bouhala, L.; Koutsawa, Y.; Karatrantos, A.; Bayreuther, C. Design of Type-IV Composite Pressure Vessel Based on Comparative Analysis of Numerical Methods for Modeling Type-III Vessels. *J. Compos. Sci.* **2024**, *8*, 40. [CrossRef]
36. Kumkam, N.; Sleesongsom, S. Reliability-Based Topology Optimization with a Proportional Topology for Reliability. *Aerospace* **2024**, *11*, 435. [CrossRef]
37. Hasan, A.; Lu, C.; Liu, W. Lightweight Design and Analysis of Steering Knuckle of Formula Student Car Using Topology Optimization Method. *World Electr. Veh. J.* **2023**, *14*, 233. [CrossRef]
38. Wang, Q.; Han, H.; Wang, C.; Liu, Z. Topological control for 2D minimum compliance topology optimization using SIMP method. *Struct. Multidiscip. Optim.* **2022**, *65*, 38. [CrossRef]
39. Yan, J.; Lin, H. Adaptive Slicing of Implicit Porous Structure with Topology Guarantee. *Comput.-Aided Des.* **2023**, *162*, 103557. [CrossRef]